



Simulating migrated seismic data by filtering an earth model: A MATLAB[®] implementation[☆]

G. Toxopeus^{a,*}, J. Thorbecke^a, S. Petersen^b, K. Wapenaar^a, E. Slob^a

^a Department of Geotechnical Engineering, Delft University of Technology, PO Box 2600 GA, Delft, The Netherlands

^b StatoilHydro Research Center, Sandstli, Bergen, Norway

ARTICLE INFO

Article history:

Received 17 August 2008

Received in revised form

9 June 2009

Accepted 15 June 2009

Keywords:

Seismic modeling

Migration image

Seismic interpretation

ABSTRACT

An earth model is used in a collaborative environment in which some members provide information for its construction and others utilize the result. Validating an earth model by simulating a migration image is an important step. However, the high computational cost of generating 3D synthetic data, followed by the process of migration, limits the number of scenarios that can be validated. To overcome this computational cost, a novel strategy is used where a migration image is simulated by filtering a model with a spatial resolution filter. One of the key properties of this approach is that the model that describes a target-zone is decoupled from the macro-velocity model that is used to compute the spatial resolution filters. Consequently, different models can be filtered with the same resolution filter. For a horizontally layered medium, the Gazdag phase-shift operators are used to construct a common-offset spatial resolution filter to simulate the phase of 2D primary reflection data. To approximate a spatial resolution filter in a laterally variant medium, ray trace information is used as an illumination constraint. Additionally, the influence of seismic uncertainties on the shape of a spatial resolution filter and the resulting migration image are simulated. These filters enhance an iterative earth modeling approach.

© 2009 Elsevier Ltd. All rights reserved.

1. Introduction

Seismic exploration activities can be subdivided into acquisition, seismic processing and interpretation. In the first stage, a network of sensors records the space–time response of the subsurface due to seismic waves generated by a controlled source. The source has a particular signature and frequency content. Next, computer algorithms are used to process the recorded data, where the principal processing step is known as migration. At this stage a seismic depth image of the target-zone is obtained. For an extensive overview of the different seismic processing steps we refer to Yilmaz (2001). Finally, in the interpretation stage, structural information can be obtained from the migration image. For an extensive overview of 3D seismic interpretation techniques we refer to Brown (2004). Seismic interpretation is not a trivial task, because of the relatively low resolution of the migration image. For example, a migration image has a typical vertical resolution of 25 m, a horizontal resolution of 50 m, and has an extensive spatial coverage (covering many km² with typical sampling distances 12.5–37.5 m in the lateral

dimension). The resolution of a migration image is controlled by the acquisition parameters, the seismic processing parameters, the overburden properties, the accuracy of the velocity model that was used to migrate the real data and the depth range of the target-zone. To understand the imprint of these effects in a migration image, migrated data are simulated by generating 3D synthetic data, followed by the process of migration. However, this approach has a very high computational cost. Therefore, it is not often used to validate an earth model. The current industry practice of simulating seismic data in the depth domain for earth modeling is the so-called 1D convolution model. In this approach a 1D wavelet, which matches the source, is used to filter an earth model to simulate a migration image. For example it is used in geological modeling by Pratson and Gouveia (2002) or Braaksma et al. (2006). This method is computationally very fast. Unfortunately, it assumes that the earth is locally horizontally layered. Therefore, the simulation result only expresses the vertical resolution of a migration image correctly for horizontal layers and does not account for the lateral resolution aspects of the migration process.

Recent research shows that a migration image can be simulated accurately and computationally efficiently by filtering a model with a spatial resolution filter (Schuster and Hu, 2000; Gjøystdal et al., 2002, 2007; Lecomte et al., 2003; Toxopeus et al., 2003a). The real migration image is obtained with a background

[☆] Code available from server at <http://www.iapg.org/CGEditor/index.htm>.

* Corresponding author.

E-mail address: GTox@StatoilHydro.com (G. Toxopeus).

¹ Present address: StatoilHydro, Drammensveien 264, N-0240, Oslo, Norway.

velocity model. This model is also used to compute a spatial resolution filter. The spatial resolution filter expresses the effects of the acquisition parameters, seismic processing parameters and the overburden. As a consequence, the simulated migration image can be compared directly to the migrated data. Under the assumption that the background velocity model remains unchanged, the spatial resolution filter stays constant and can be reused to simulate migration images of different geological scenarios (Toxopeus et al., 2008).

In this paper a forward modeling and migration scheme is proposed for calculating spatial resolution filters in a velocity model. For this purpose, we first show an example to illustrate how we simulate a migration image by filtering an earth model with a spatial resolution filter. This is followed by a discussion about the Gazdag phase-shift operators and an implementation in MATLAB. Next, we approximate a spatial resolution filter in a laterally variant medium by using ray-trace information as illumination constraint and demonstrate the influence of seismic uncertainties. Finally, a common-offset spatial resolution filter is computed. The presented examples are in 2D and simulate the phase of primary reflection data only, however, the approach is valid in 3D for an arbitrary elastic earth model. The numerical implementation is done in MATLAB, so that it can be used as a teaching tool as well (Toxopeus et al., 2003b).

2. Simulating a migration image

For seismic exploration on sea, a ship drags an airgun source and a finite number of detectors (hydrophones) through the water (a simplified 2D illustration is shown in Fig. 1). At regular intervals, the source generates a wavefield. This wavefield travels into the earth and partly reflects at different layers due to impedance contrasts. Acoustic impedance is the product of density and velocity, the ratio of the pressure to the volume displacement at a given surface in a sound-transmitting medium (Sheriff, 2001). The impedance contrast directly relates to the reflection amplitude. At the surface, using different detector positions, the reflected wavefield is recorded in time. Along the course of the ship, the seismic experiment is repeated for many source positions. A similar type of experiment can be performed for exploration on land, with the airguns replaced by seismic vibrators or dynamite and the hydrophones replaced by geophones. For shallow targets on land, a ground penetrating radar (GPR) that emits electromagnetic waves can also be used. On a conceptual level, the acquired data of these wavefield

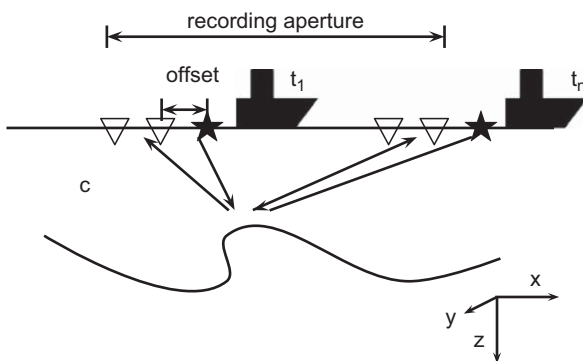


Fig. 1. A schematic illustration of seismic data acquisition at two different times (t_1 and t_n) on sea. A wave propagation velocity is denoted by c , \star is a source at different lateral positions and ∇ is a detector. Arrows illustrate paths that a primary wavefield travels between a source, a geological boundary (curved solid line) and different detectors (hydrophones) in water.

experiments (seismic or electromagnetic) are described as

$$\text{Real data}(\mathbf{x}_D, \mathbf{x}_S, t) = \text{Physical measurement}\{\text{Earth}\}, \quad (1)$$

where \mathbf{x}_D and \mathbf{x}_S denote the 3D spatial coordinate vectors of the detector and source positions, respectively, and t denotes time. Similarly, the simulated seismic data are obtained by a forward operator that acts on an earth model. The earth model is a possible representation of the earth in terms of the parameters dominating the measurements used, while the forward operator resembles our description of the physical measurement, according to

$$\text{Simulated data}(\mathbf{x}_D, \mathbf{x}_S, t) = \text{Forward operator}\{\text{Earth model}(\mathbf{x})\}, \quad (2)$$

where \mathbf{x} denotes the spatial coordinate vector of position in the earth model. From the seismic measurements, a structural depth-image of the earth is obtained by using a migration operator. This extends the relations to

$$\text{Real migration image}(\mathbf{x}) = \text{Migration operator}\{\text{Real data}(\mathbf{x}_D, \mathbf{x}_S, t)\},$$

$$\text{Simulated migration image}(\mathbf{x}) = \text{Migration operator}\{\text{Simulated data}(\mathbf{x}_D, \mathbf{x}_S, t)\}. \quad (3)$$

The interpreter of the migration image is concerned with the question how and to what extent geological details are visible in the migration image. Ideally he or she should investigate the following relations:

$$\text{Real migration image}(\mathbf{x}) = \text{Migration operator}\{\text{Physical measurement}\{\text{Earth}\}\},$$

$$\text{Simulated migration image}(\mathbf{x}) = \text{Migration operator}\{\text{Forward operator}\{\text{Earth model}(\mathbf{x})\}\}. \quad (4)$$

These are the combined operations of the aforementioned processes. Therefore, to simulate migrated data, a combined operator is introduced to represent the two operators,

$$\text{Simulated migration image}(\mathbf{x}) = \text{Combined operator}\{\text{Earth model}(\mathbf{x})\}, \quad (5)$$

where

$$\text{Combined operator}\{\cdot\} = \text{Migration operator}\{\text{Forward operator}\{\cdot\}\}. \quad (6)$$

The combined operator is represented by a spatial resolution filter that is obtained from computing the image of a single unit strength scattering point in a background medium (the impulse response is the filter). Eq. (5) describes an efficient way of simulating a migration image. It can be used to validate different earth model scenarios by comparing the simulated migration images with the real migration image of Eq. (3).

In the literature, a spatial resolution filter is also known as a point-spread function (PSF) (Devaney, 1984; Jansson, 1997; Lecomte and Gelius, 1998; Gjøystdal et al., 2002), the Green's function for migration (Schuster and Hu, 2000) or resolution function (Lecomte and Gelius, 1998). To illustrate the new approach of simulating migrated data, a reflectivity model of an extended wedge model is shown in Fig. 2(a). The model has different dips. A wedge model is commonly used to study petroleum reservoirs (Widess, 1973), the model represents a common stratigraphic petroleum trap (Norman, 2001). The simulated migration image, given a certain acquisition configuration (seismic imprint), is shown in Fig. 2(b). The image

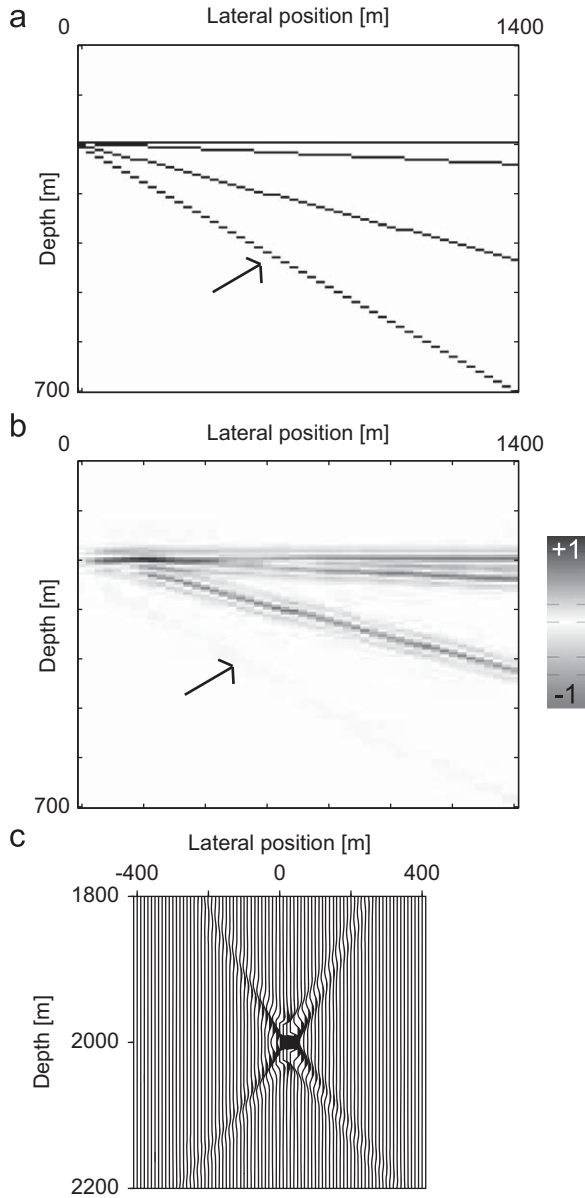


Fig. 2. (a) Illustration of a model. (b) Simulating a depth-migration image by filtering an earth model with a spatial resolution filter (c). Layers are blurred in both vertical and horizontal directions, making them difficult to interpret especially where they are close to each other. Additionally, the steepest dip is suppressed, illustrated by an arrow. Similar effects occur in migrated real data and hamper geological interpretation.

is obtained using the spatial resolution filter shown in Fig. 2(c) through a 2D spatial convolution with the reflectivity model.

In the following we briefly highlight four aspects of this new concept of simulating migrated data. More background information is found in Toxopeus et al. (2008). First, the spatial resolution filter depends on depth and lateral position. Ideally, for each subsurface point a new spatial resolution filter could be computed. However, this is computationally too expensive. Fortunately, for a small area, the spatial resolution filter can be assumed constant. A target-oriented illumination analysis based on ray-tracing, or the full-wave equation, could be used to investigate the degree of lateral variation of the spatial resolution filter. Examples are found in Lecomte (2006) and Yang et al. (2008). Second, the spatial resolution filter can be decoupled from

the geologically more detailed earth model describing the target-zone. The propagation model that is used to migrate the real data is also used to compute the spatial resolution filter. This velocity model is not changed and therefore the spatial resolution filter can be re-used to validate different geological scenarios. Third, a spatial resolution filter is computed in depth, because an earth model is also built in depth. To compute a time-migration image, a depth-to-time conversion can be performed. Finally, all effects related to the acquisition and Earth surface can be properly captured in the spatial resolution filter. As an initial approach, a spatial resolution filter only simulates (the phase of) migrated reflection data given an overburden model, and acquisition and processing parameters. In the comparison between the real and simulated data, it is tacitly assumed that all multiple scattering events have been properly removed from the real data or imaged to their correct position of origin. Removing multiple energy is of great importance in seismic processing and the current industry practice is to remove only the free surface scattering from the real data; internal multiple scattering is only partly removed (Verschuur et al., 1992; Hill et al., 1999; Matson and Dragoset, 2005).

3. Computing a spatial resolution filter in a horizontally layered velocity model

Three approaches to calculating a spatial resolution filter are found in the literature. The first approach assumes a homogeneous velocity model; Chen and Schuster (1999) presented a closed-form expression for the zero-offset case. Second, for a 3D elastic model, directional information can be derived using ray-tracing (Lecomte and Gelius, 1998; Lecomte, 2008) or it is obtained by a local plane-wave analysis (Xie et al., 2006). The third approach uses the combined operator of relation (5). In the following discussion, we will use this latter approach and further restrict ourselves to the 2D case, a horizontally layered velocity model and show examples for primary reflection data only. The layered model is built from a velocity trace that is obtained from, e.g., a borehole or from the migration velocity model that was used to migrate the seismic real data. In each layer, the velocity is constant and a wavefield is propagated in this layer by making use of the Gazdag phase-shift operator (Gazdag, 1978). In the double-Fourier domain, or k_x, ω domain it reads

$$\tilde{W}^-(z_{m-1}, z_m) = e^{-jk_z|z_{m-1} - z_m|} \quad (7)$$

with

$$k_z = \begin{cases} \sqrt{k^2 - k_x^2}, & k_x^2 \leq k^2, \\ -j\sqrt{k_x^2 - k^2}, & k_x^2 > k^2, \end{cases}$$

where $j = \sqrt{-1}$, $k = \omega/c$, ω is the radial frequency, c is the P-wave velocity and k_x is the Fourier-transformed horizontal spatial coordinate. The depth is denoted by z and z_m denotes the m th sample of the gridded input velocity trace.

For upward propagating waves, the operator of Eq. (7) is used to propagate the wavefield P at depth z_m one layer higher:

$$\tilde{P}^-(z_{m-1}) = \tilde{W}^-(z_{m-1}, z_m) \tilde{P}^-(z_m). \quad (8)$$

Eq. (8) is used in a recursive scheme to propagate the wavefield from z_M to z_0 . The recursion starts at the depth level for which one wants to derive the spatial resolution filter (z_M), with $\tilde{P}^-(k_x, z_M, \omega) = S(\omega)$, $S(\omega)$ being the source spectrum, and ends at the acquisition level z_0 , giving the impulse response of the source at z_M .

We assume that a migration image approximates migrated zero-offset data. Zero-offset data are obtained by moving a coinciding source and detector along the acquisition surface

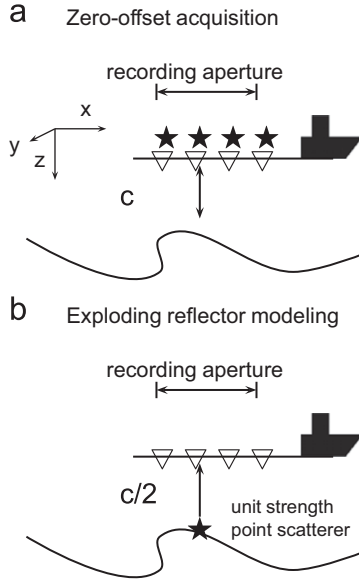


Fig. 3. (a) A real experiment for a zero-offset case. (b) Simulating zero-offset case by exploding reflector model for one unit strength scattering point. A wave velocity is denoted by c , \star is a source at different lateral position and ∇ is a detector. An arrow illustrates paths that a primary wavefield travels between a source, a geological boundary (curved solid line) and different detectors in water.

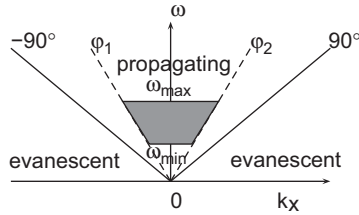


Fig. 4. An overview of wave-propagation in double-Fourier domain. A horizontal axis displays wavenumber (k_x) and vertical axis angular frequency ($\omega = 2\pi f$). Solid lines (denoted by -90° and 90°) mark boundary between propagating and evanescent part of a wavefield. A dashed lines indicate minimum and maximum angles of wave propagation (φ_1 and φ_2). These angles are in general less than 90° due to a limited recording aperture and effects of overburden. A signal of artificial source has a frequency content that is marked by ω_{\min} to ω_{\max} . To reduce computational costs only gray filled region is computed.

(Fig. 3(a)). This recording geometry is not realizable in practice for seismic exploration. However, we still need to migrate the recorded data to zero-offset to get the reflectors at proper dips and collapse hyperbolic events of scattering objects to “points”. We consider an alternative modeling approach that approximates zero-offset data, the so-called exploding reflector modeling approach (Loewenthal et al., 1976; Yilmaz, 2001). In this approach, sources are placed at the reflectors and the source strengths are chosen proportional to the reflection coefficients. The propagation velocity in the model taken to be half the actual velocity. Hence, we replace $k = \omega/c$ by $k = 2\omega/c$. When all sources “explode” simultaneously, data are obtained that resemble zero-offset data (Fig. 3(b)). To obtain forward modeled data for a spatial resolution filter, one source with unit strength is placed in a background model.

This is step one in the computation of a spatial resolution filter. To obtain the filter, the forward modeled impulse response is migrated. The inverse wavefield extrapolator ($\tilde{F}^- = 1/\tilde{W}^-$) forms the basis for migration. To obtain a stable inverse wavefield extrapolator, the complex conjugate of the forward operator is taken according to $\langle \tilde{F}^- \rangle = (\tilde{W}^-)^*$. Physically, this means that

only the propagating wave region (for which $k_x^2 \leq k^2$) is used (as indicated in Fig. 4). Hence,

$$\langle \tilde{P}^- (z_m) \rangle = \langle \tilde{F}^- (z_m, z_{m-1}) \rangle \langle \tilde{P}^- (z_{m-1}) \rangle, \quad (9)$$

where

$$\langle \tilde{F}^- (z_m, z_{m-1}) \rangle = e^{+jk_z^* |z_m - z_{m-1}|} \quad (10)$$

with

$$k_z^* = \begin{cases} \sqrt{k^2 - k_x^2}, & k_x^2 \leq k^2, \\ j\sqrt{k_x^2 - k^2}, & k_x^2 > k^2 \end{cases} \quad (11)$$

and $\langle \tilde{P}^- \rangle$ is the backward propagated wavefield.

The migration image is obtained by evaluating the wavefield in the space–time domain at $t = 0$ for all depth levels. In the double-Fourier domain this is done by a summation over all frequency components for each k_x . Finally, the spatial resolution filter is obtained by an inverse Fourier transformation from the wave-number (k_x) to the space domain,

$$\text{Spatial resolution filter}(x, z) = \Re \int_{k_x = -\infty}^{k_x = \infty} e^{-jk_x x} \int_{\omega_{\min}}^{\omega_{\max}} \langle \tilde{P}^- (k_x, z, \omega) \rangle d\omega dk_x, \quad (12)$$

where x, z denote the spatial coordinates of a point in the earth model. We take only the real part (\Re) of the equation, because the real part is used as the imaging condition for zero-offset data. For more extensive details of wavefield propagation we refer to Berkhout (1987) and Wapenaar and Berkhout (1989).

Finally, we remark that the Gazdag operators are not commonly used in the seismic industry to migrate real data, because they fail to properly image complex velocity structures, as for example, in a salt body. Depth migration and modeling algorithms for a complex velocity model are freely available from, for example, Colorado School of Mines (Seismic Un*x Stockwell, 1999; Forel et al., 2006) and the University of Calgary (CREWES project Margave, 2001). By replacing the one-way Gazdag operators by spatially variant one-way operators that are valid for a more complex velocity model, a more accurate spatial resolution filter can be computed using the same two steps.

3.1. Numerical implementation

Consider the following four features of the Gazdag phase-shift operator that make an implementation computationally efficient. First, if the square root in the phase-shift operator becomes imaginary the wavefield is evanescent (exponentially decaying). Therefore, the phase-shift operator is only applied if the wavefield is propagating (i.e., for real-valued square-root). The minimum and maximum angles of wave propagation (φ_1 and φ_2) mark the boundaries (Fig. 4). These are less than 90° due to a limited recording aperture and effects of the overburden. In the wave-number domain, the minimum and maximum angles of wave propagation restrict the domain as $k_1 < k_x < k_2$, with $k_{1,2} = k \sin(\varphi_{1,2})$. Second, the signal of the controlled source has a particular frequency content from ω_{\min} to ω_{\max} , where $\omega = 2\pi f$ and f is the frequency. This means that in the frequency range up to the Nyquist frequency, not all frequency components need to be calculated. Only the gray filled region in Fig. 4 needs to be evaluated. Third, note that applying the phase-shift operator is a linear process. The phase-shift operator can be re-used to propagate the wavefield one depth-level if the velocity is constant. Finally, either a loop over ω or k_x is removed by making use of the matrix multiplication possibilities which are specific to MATLAB.

Modeling is performed on a discretized k_x -axis, after an inverse Fourier transform. This gives periodic results in the spatial domain. These periodic effects can be partly avoided by enlarging

the modeling domain, and after inverse Fourier transform only selecting the least disturbed spatial domain of interest in the middle of the spatial period. As a rule of thumb it is usually sufficient to enlarge the recording aperture by a factor of two. Another well known technique is to taper the edges of the forward modeled data at each depth-level (Cerjan et al., 1985). The computational costs of the modeling algorithm are then increased, because applying the tapers requires an inverse- and a forward spatial Fourier transform at each depth-step.

3.2. Algorithms

Input to the forward algorithm is a gridded velocity trace, the depth of the unit strength point scatterer, and information on the acquisition and processing parameters. The main acquisition parameter is the recording aperture. It is used to truncate the forward modeled data to the acquisition aperture. One of the main processing parameters is the total number of samples (denoted by nt), which is computed by dividing the total recording time by the time sampling (denoted by dt). Additionally, information on the minimum and maximum angles of wave propagation is used to constrain the shape of the spatial resolution filter. A specifically shaped source wavelet is convolved

with the modeled data after forward modeling. All these input parameters should resemble the acquisition and processing parameters of the real data as closely as possible in order to simulate a migration image that can be directly compared to a real migration image.

The P-wave velocity is divided by two and is used to model primary zero-offset reflection data. The classic algorithm for forward modeling using the Gazdag one-way operator (relation (8)) is illustrated in Fig. 5. The primary reflection data are truncated to their original recording aperture. On a trace-by-trace basis, a specific source wavelet is convolved with the data by a multiplication in the frequency domain. The classic algorithm for migrating seismic data using the Gazdag one-way operator (relations (9) and (12)) is illustrated in Fig. 6. Note that the depth loop ends at a larger depth (z_d) than the depth (z_0) of the point scatterer, to obtain a two-sided spatial resolution filter.

4. Approximating the spatial resolution filter in a laterally variant medium

A point scatterer is located in a model with a velocity of 2000 m/s at $x=1500$ m, $z=2000$ m. A zero-offset acquisition setup is placed symmetrically over the location. The total

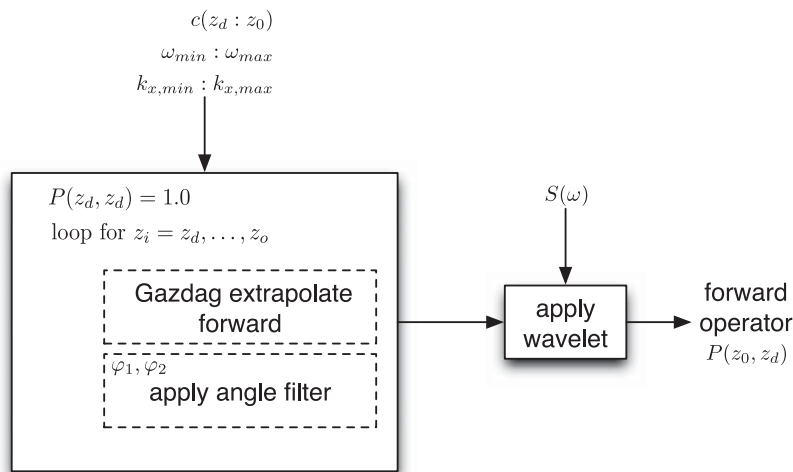


Fig. 5. Classic implementation of zero-offset seismic modeling using one-way forward operator and exploding reflector concept (relation (8)). In this paper the Gazdag operator is used as one-way operator. A + and – sign denotes forward and backward propagations, respectively.

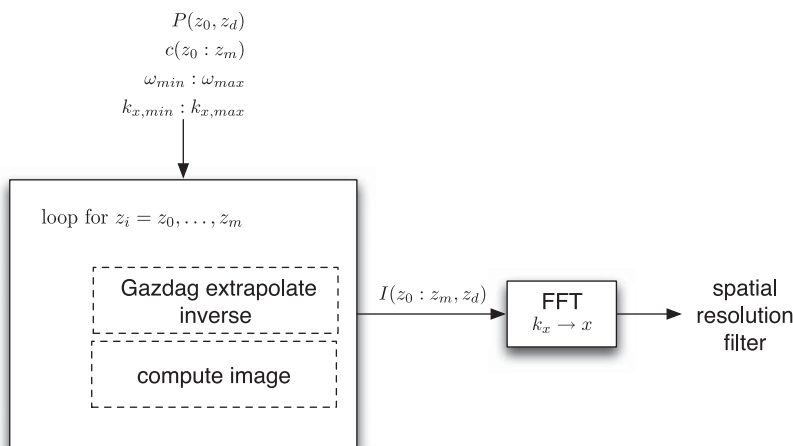


Fig. 6. Classic implementation of migrating seismic data using a one-way operator (relations (9) and (12)). In this paper the Gazdag operator is used. Migrating forward modeled data of a point scatterer results in a spatial resolution filter. A + and – sign denotes forward and backward propagations, respectively.

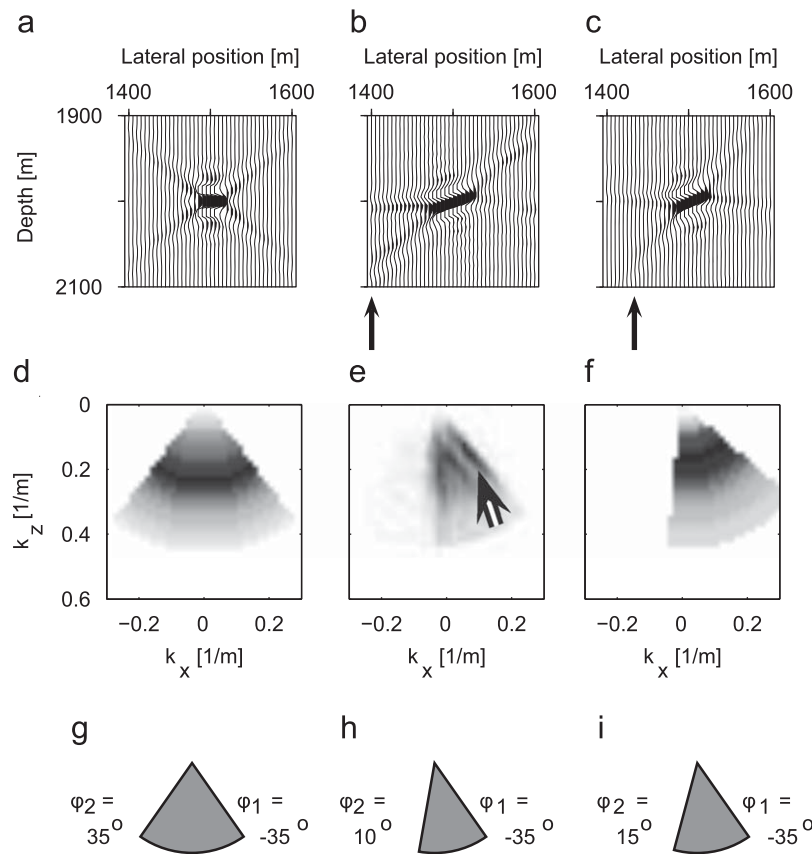


Fig. 7. Different spatial resolution filters at position $x = 1500$ m, $z = 2000$ m. (a) Spatial resolution filter derived in a homogeneous model of 2000 m/s. (b) Spatial resolution filter in simple salt model using $x - \omega$ operators. (c) A local constant velocity spatial resolution filter in simple salt model. (d)–(f) Double-Fourier transformed results of figure (a)–(c). (g)–(i) Schematically illustrate measured minimum and maximum angles of wave propagation in double-Fourier domain.

recording aperture is 3000 m. The source signature is a Ricker wavelet with a sampling of 4 ms. The signal of the wavelet is characterized by a center frequency at 25 Hz. Using the Gazdag phase-shift operator a spatial resolution filter is computed (Fig. 7(a)). Next, a water layer and a strong velocity contrast are added to the model, which creates the simple-salt-model shown in Fig. 8(a). These structures are for example found in the Gulf of Mexico (Jackson et al., 1994). Note that the phase-shift approach is not valid in the laterally variant medium. Therefore, the spatial resolution filter is computed using space–frequency domain operators. These are valid in a complex velocity medium (Thorbecke et al., 2004). This spatial resolution filter is shown in Fig. 7(b). We refer to this filter as the reference case. Although the same acquisition setup is used, the shape of the spatial resolution filters obtained from the homogenous and complex model, differs significantly (Figs. 7(a) and (b)). This has an important influence on the interpretation of the simulated migration images. The shape of the spatial resolution filter determines which reflectors are suppressed and which remain on a migration image (Lecomte, 2008; Toxopeus et al., 2008). To approach the reference case using the Gazdag phase-shift operator, an additional constraint is needed. This information is obtained by ray-tracing (Lambará et al., 1996), through a smoothed version of the velocity model (Fig. 8(b)). We find that the minimum and maximum angles of wave propagation as seen by ray-tracing are $\varphi_1 \sim -35^\circ$ and $\varphi_2 \sim 15^\circ$, which is illustrated in Fig. 8(b). These angles are used as a constraint to the forward modeling of the Gazdag operators in a layered velocity model constructed with the aid of the velocity trace at $x = 1500$ m of the simple salt model. This spatial resolution

filter is shown in Fig. 7(c). We name it a local constant-velocity spatial resolution filter, because the spatial resolution filter is obtained under a “local constant-velocity” assumption. The filter shows a strong resemblance (regarding the phase) with the reference result. However, as indicated by the black arrows in Figs. 7(b) and (c), the shape of the filter is slightly different from the reference case. This is also expressed in the double-Fourier domain, where the minimum and maximum angles of wave propagation for the $x - \omega$ spatial resolution filter are $\varphi_1 \sim -35^\circ$ and $\varphi_2 \sim 10^\circ$. Thus, the φ -range obtained by ray-tracing is about 5° too wide. Another difference between the two is that in the double-Fourier domain the reference filter shows an amplitude dip between the minimum and maximum angles of wave propagation, indicated by the double arrow in Fig. 7(e). Initially, for the local constant velocity spatial resolution filter it is assumed that between φ_1 and φ_2 all angles are present, an amplitude dip is not taken into account. However, constructing a spatial resolution filter is a linear process. In order to take the amplitude dip into account, two spatial resolution filters can be computed such that an “illumination gap” is created when the filters are added. Note that a spatial resolution filter in a laterally variant model is constructed directly from directional information obtained from either ray-trace information (Lecomte and Gelius, 1998; Lecomte, 2008) or by a local plane-wave analysis of a one-way wavefield (Xie et al., 2006). Finally, the spatial resolution filter is used to simulate a migration image of a model with two dips at $\pm 15^\circ$ and $\pm 45^\circ$ (Fig. 9). The resulting image only shows one reflector, the other reflectors are suppressed, which hampers geological interpretation in a complex setting and shows the need

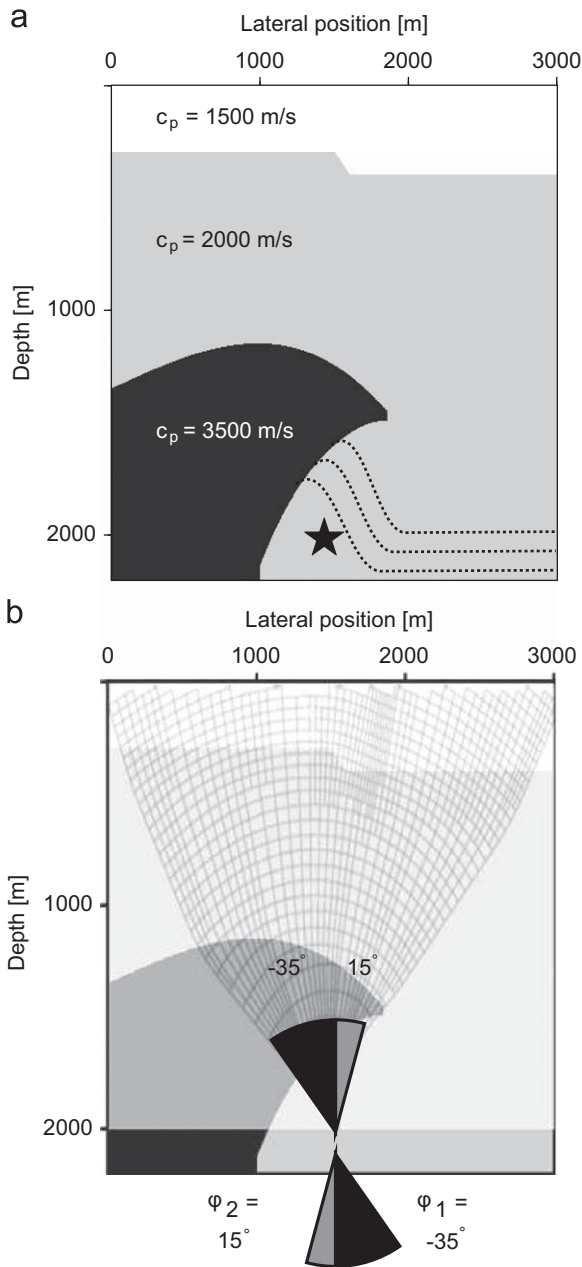


Fig. 8. (a) A simple salt-model. An asterisk denotes position of spatial resolution filter. A structure that could trap hydrocarbons at flank of salt is shown by dashed lines. This structure is validated in Fig. 9. (b) A ray-tracing result is overlying simple salt-model. (c) Schematically illustrated are minimum and maximum angles of wave propagation that are obtained by ray-tracing, figure (b).

for an improved survey design in order to illuminate the subsurface. A real data example that uses a local constant-velocity spatial resolution filter to validate a geological model is shown in Toxopeus et al. (2008).

4.1. Studying seismic uncertainties

In the previous discussion it has been shown that the shape of a spatial resolution filter is mainly controlled by the source wavelet and the maximum angle of wave propagation. However, it was tacitly assumed that all seismic processing steps could be ideally performed. For example, to properly perform migration, a velocity model of the subsurface is needed, and the effect of statics has to be removed from the recorded data (Yilmaz, 2001).

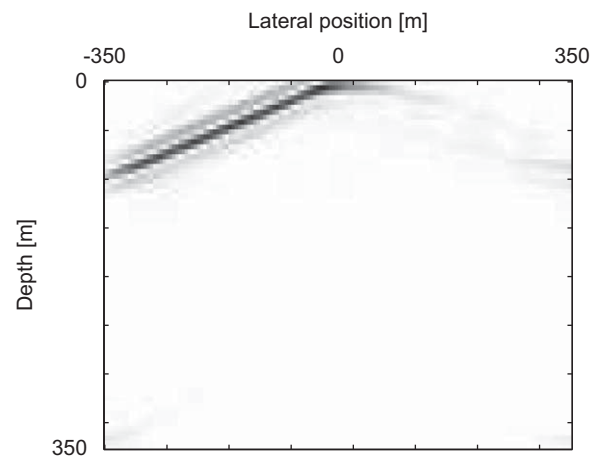


Fig. 9. Simulated migration image of a reflectivity model with dips at $\pm 15^\circ$ and $\pm 45^\circ$. A pyramid model illustrates two different realizations of possible trap structure near a salt (dashed lines in Fig. 8). A colorbar is shown in Fig. 2(b).

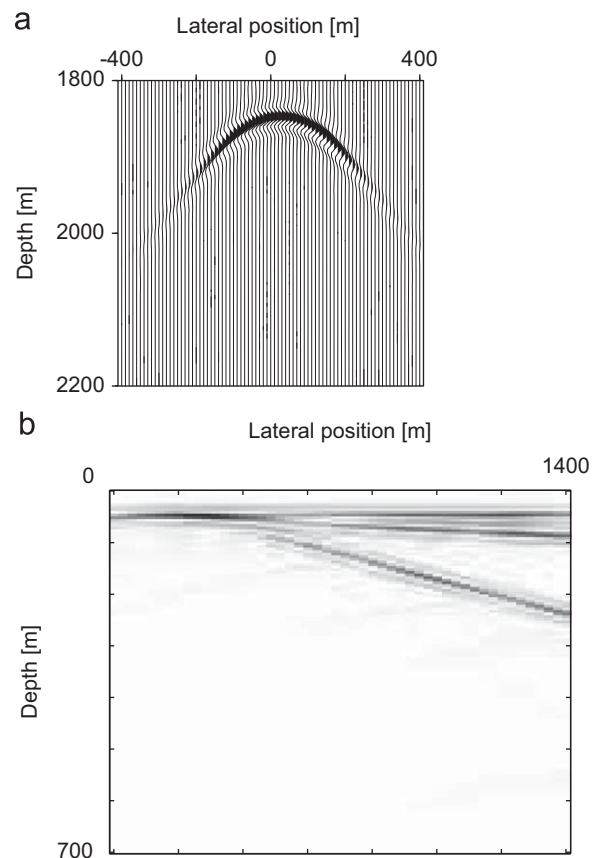


Fig. 10. (a) Simulating seismic uncertainties by filtering an earth model (Fig. 2(a)) with a suboptimal focused spatial resolution filter (figure (b)). A filter is computed using a forward model with $c = 2000$ m/s and migration model with $c = 1850$ m/s. Compare Figs. 2(b) and figure (a) and observe that migration image is more smeared and shifted upwards.

The examples in this section demonstrate how seismic uncertainties influence the shape of a spatial resolution filter and consequently a migration image.

4.1.1. Influence of the background velocity model

Finding a background velocity model to properly migrate the recorded seismic data is not an easy task. Migrating seismic

recordings with a wrong velocity model results in events that are not properly focused and not positioned at the proper spatial position, both laterally and vertically (Toxopeus et al., 2008). A migration velocity model that is 10% lower than the modeling velocity produces a suboptimally focused spatial resolution filter. By filtering the earth model of Fig. 2(a) with the suboptimal-focused spatial resolution filter (Fig. 10(a)), a suboptimal-focused migration image is simulated (Fig. 10(b)). The filter is also known as a migration frown (Zhu et al., 1998). The suboptimally focused migration image is more smeared and the depth position of the target zone is wrong compared to the focused migration image (compare Figs. 2(b) and 10(b)).

4.1.2. Influence of statics

In practice, a static correction is applied to the seismic recordings to correct for the effects of, e.g., variations of elevation (Sheriff, 2001). In order to simulate the effect of not correctly removing statics on migrated data, the forward modeled data (obtained as illustrated in Fig. 5) are trace-by-trace randomly shifted by 0 or ± 4 ms. The time-shifts represent statics. The shifted data are migrated (as shown in Fig. 6). The resulting spatial resolution filter is shown in Fig. 11. The filter shows a number of migration tails that have not properly canceled out against each other (Hagedoorn, 1954). This filter can be used to simulate a migration image that shows how statics may hamper

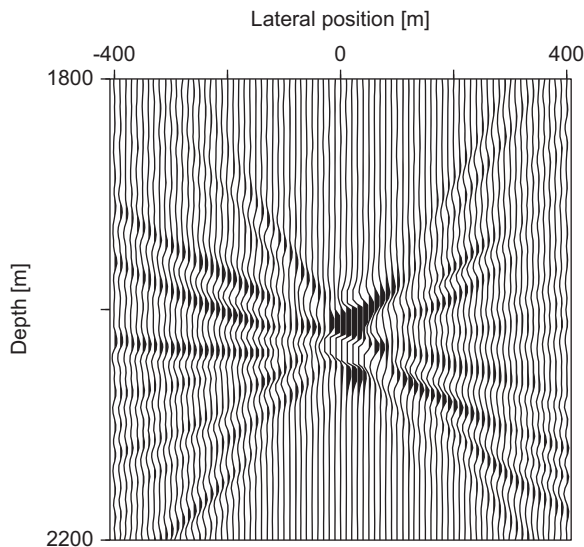


Fig. 11. A spatial resolution filter after statics are introduced.

interpretation of (time-lapse) seismic measurements. An example of a migration image of a wedge model with and without statics is shown in Figs. 12(a) and (b), respectively. The difference image shows that uncertainties are introduced in the interpretation of the top or base if statics are not corrected handled in the input data or migration (Fig. 12(c)).

5. A common-offset spatial resolution filter

Different stacks of common-offset data (Fig. 1), commonly denoted as mid, near and far, provide amplitude information in fluid and rock classification (Yilmaz, 2001; Avseth et al., 2003). In order to simulate amplitude information of a migration image, a proper reflectivity model and spatial resolution filter are needed. The reflectivity model is obtained by calculating the incident angle associated with the offset. A quick approach would be to use Snell's law to find the incidence angle on a trace-by-trace basis, which is a common technique to transform an offset- to angle-image. A spatial resolution filter for a specific offset is computed using the following steps. First, instead of using half the modeling velocity, the initial modeling velocity is used as input to the presented forward modeling algorithm. This results in propagating primary data for a given buried point scatterer location. These data are denoted as one-way time data. An example for a homogeneous velocity model of 2000 m/s and a point scatterer at a depth at 1500 m is shown in Fig. 13(a). Next, one offset is chosen and the associated source (S) and detector (D) paths are selected from the modeled data. By convolving the two selected one-way datasets (one for the source- and one for the receiver-offset), two-way data for one common-offset is computed (Fig. 13(b)). Note that this method is valid for an arbitrary elastic model (Deregowski and Rocca, 1981)). Finally, these data are convolved on a trace-by-trace basis with a specific source signature that resembles the artificial source of the real seismic experiment.

Migrating common-offset data using the one-way Gazdag operator is not straightforward. A diffraction-summation type migration method or an approximation, i.e., the stationary phase, can be used to perform common-offset migration (Popovici, 1994; Yilmaz, 2001). Here we migrate the input data using two-way operators, where we make use of the fact that the migration operator is laterally invariant in a layered medium (Streich et al., 2007). The depth-loop is limited to a depth-range around the depth location of the unit point scatterer. To migrate common-offset data, a similar illustration as shown in Fig. 6 is used, but the one-way operator is replaced by a two-way Gazdag operator. Alternatively, a common-offset spatial resolution filter in a

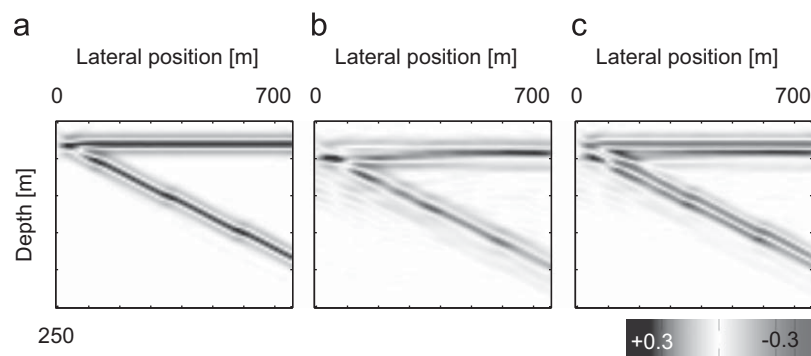


Fig. 12. Simulated migration image of a wedge model without (a), and with statics (b). A spatial resolution filter with statics is shown in Fig. 11. A colorbar is shown in 2(b). (c) A difference image between (a) and (b).

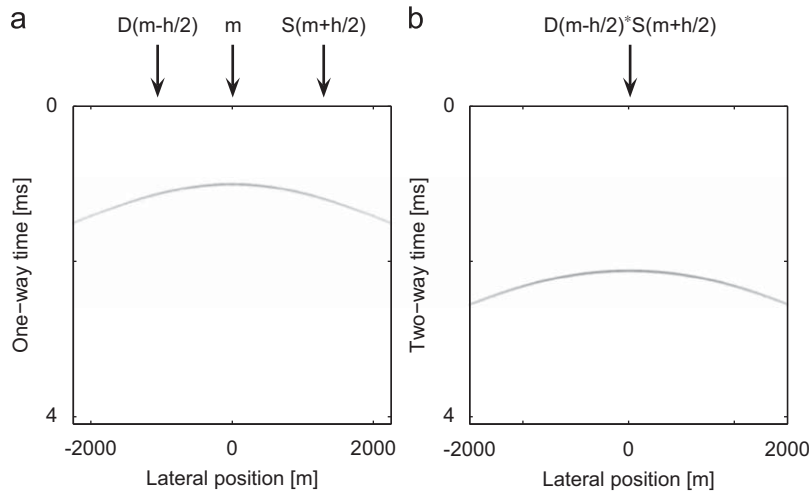


Fig. 13. (a) A one-way travel time of a unit strength point scatterer at position $x = 0$ m and $z = 2000$ m recorded with a recording aperture of 1500 m in a homogeneous model with P-wave velocity of 2000 m/s. A detector, a source and a midpoint position are denoted by D, S, and m, respectively for a selected offset (h). (b) A common-offset data are simulated by convolving different source and detector paths.

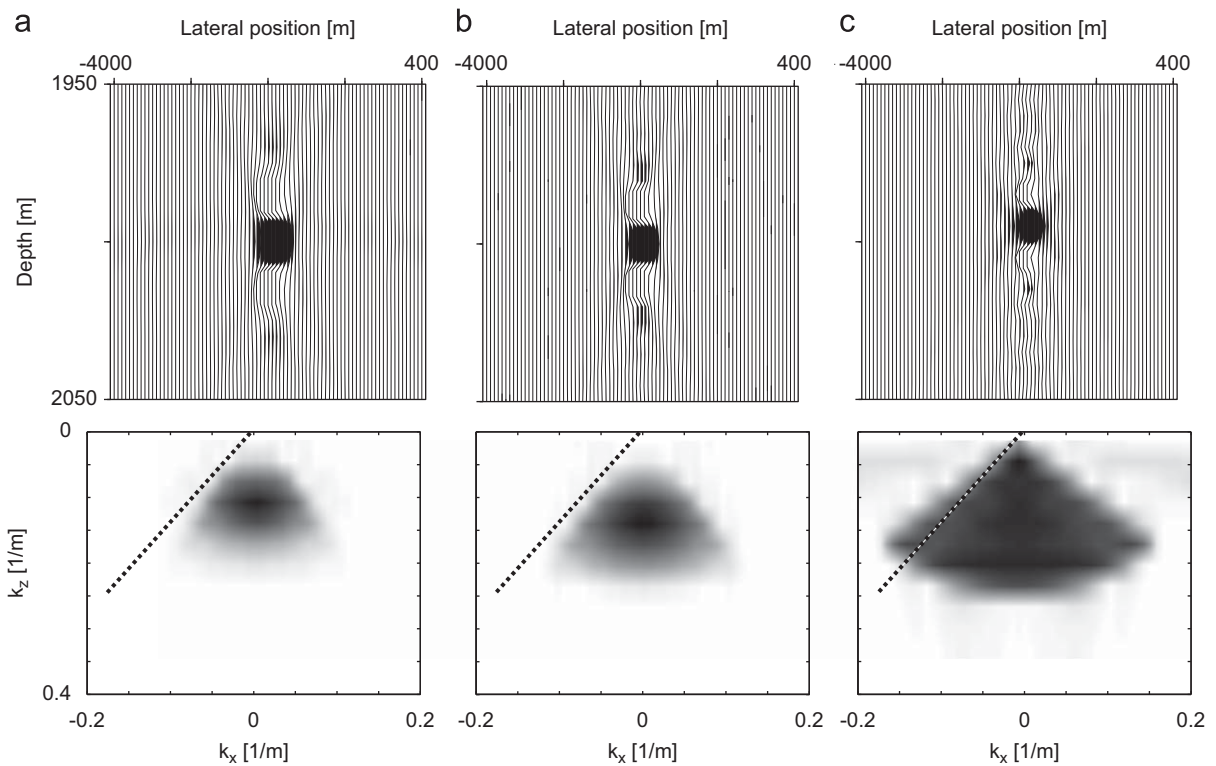


Fig. 14. Three different spatial resolutions computed in a homogeneous model. An aperture of 4500 m is used for all cases. (a) A 1500 m common-offset spatial resolution filter obtained with phase-shift operators. (b) A 1500 m common-offset spatial resolution filter obtained from a standard prestack depth-migration algorithm. (c) A zero-offset spatial resolution filter.

laterally variant model can be constructed directly from directional information obtained from either ray-trace information (Lecomte and Gelius, 1998; Lecomte, 2008) or by a local plane-wave analysis of a one-way wavefield (Xie et al., 2006).

In a homogeneous model with a P-velocity of 2000 m/s, a common-offset spatial resolution filter is computed at a depth of 2000 m. The offset is fixed at 1500 m, and the result after forward modeling and migration using the proposed algorithms, is shown in Fig. 14(a). For reference, a prestack depth-migration algorithm based on space-frequency operators is used to migrate the same forward data on a trace-by-trace basis

(Fig. 14(b)). The match regarding the phase between the two spatial resolution filters is high (compare Figs. 14(a) and (b)). Finally, for the same aperture, a zero-offset spatial resolution filter is computed (Fig. 14(c)). The minimum and maximum angles of wave propagation are almost 90° .

6. Conclusions and discussion

For the validation of a geological model, we simulate a migration image by filtering the model with a spatial resolution

filter. The spatial resolution filter is re-used to test different geological scenarios. A computationally efficient numerical implementation to simulate the phase of 2D primary reflection data, using one-way (Gazdag) wave propagators, was proposed to compute a zero-offset spatial resolution filter. In this fast approach the effect of seismic uncertainties could be easily included. These filters enable validation of different earth models. Note that amplitude effects were not studied and can also not be studied using the Gazdag operator. To approximate a zero-offset spatial resolution filter in a laterally invariant medium, ray-trace information is used as a constraint on the minimum and maximum angles of wave propagation. This latter spatial resolution filter is named a local constant velocity spatial resolution filter, because the spatial resolution filter is computed under a “local constant velocity” assumption. A comparison with a reference case shows that the shape is reasonably well approximated, however, the limitations of ray-tracing should be kept in mind. A common-offset spatial resolution filter in a layered medium was computed making use of the fact that the Gazdag phase-shift operators are shift invariant. The filters show a strong phase resemblance with the reference results. It has been demonstrated how seismic uncertainties caused by errors in migration velocities and statics change the shape of the spatial resolution filter and thus the migration image. Finally, note that the used Gazdag operators can be replaced by spatially variant one-way operators that are valid for a more complex velocity model. Additionally, other computationally more efficient implementations exist based on using directional information to construct (offset-dependent) spatial resolution filters directly.

Acknowledgments

The research reported in this paper has been financially supported by StatoilHydro. This support is gratefully acknowledged. We thank J. Stockwell for taking care of the Seismic Un*x package. Finally, we thank the reviewers Isabelle Lecomte and an anonymous reviewer for many suggestions that have improved this paper.

Appendix A. Supplementary data

Supplementary data associated with this article can be found in the online version at doi:[10.1016/j.cageo.2009.06.012](https://doi.org/10.1016/j.cageo.2009.06.012).

References

- Avseth, P., Flesche, H., Van Wijngaarden, A., 2003. AVO classification of lithology and pore fluids constrained by rock physics depth trends. *The Leading Edge* 22 (10), 1004–1011.
- Berkhout, A.J., 1987. *Applied Seismic Wave Theory*. Elsevier Science, Amsterdam, New York 380pp.
- Braaksma, H., Proust, J.N., Kenter, J.A.M., Drijkoningen, G.G., Filippidou, N., 2006. Sedimentological, petrophysical, and seismic characterization of an Upper Jurassic shoreface-dominated shelf margin (the Boulonnais Northern France). *Journal of Sedimentary Research* 76 (1), 175–199.
- Brown, A.R., 2004. *Interpretation of Three-Dimensional Seismic Data*, sixth ed. American Association of Petroleum Geologists, Tulsa, OK, USA, 514pp.
- Cerjan, C., Kosloff, D., Kosloff, R., Reshef, M., 1985. A nonreflecting boundary condition for discrete acoustic and elastic wave equations. *Geophysics* 50 (4), 705–708.
- Chen, J., Schuster, G.T., 1999. Resolution limits of migrated images. *Geophysics* 64 (4), 1046–1053.
- Deregowski, S.M., Rocca, F., 1981. Geometrical optics and wave theory of constant offset sections in layered media. *Geophysical Prospecting* 29 (3), 374–406.
- Devaney, A.J., 1984. Geophysical diffraction tomography. *Transaction on Geoscience and Remote Sensing* 22 (1), 3–13.
- Forel, D., Benz, T., Pennington, W.D., 2006. *Seismic Data Processing with Seismic Un*x*, first ed. Society Of Exploration Geophysicists, Tulsa, OK, USA, 273pp.
- Gazdag, J., 1978. Wave equation migration with the phase-shift method. *Geophysics* 43 (7), 1342–1351.
- Gjøystdal, H., Iversen, E., Laurain, R., Lecomte, I., Vinje, V., Astebol, K., 2002. Review of ray theory applications in modelling and imaging of seismic data. *Studia Geophysica et Geodætica* 46 (2), 113–164.
- Gjøystdal, H., Iversen, E., Lecomte, I., Kaschwich, T., Drottning, Å., Mispel, J., 2007. Improved applicability of ray tracing in seismic acquisition, imaging, and interpretation. *Geophysics* 72 (5), SM261–SM271.
- Hagedoorn, J., 1954. A process of seismic reflection interpretation. *Geophysical Prospecting* 2, 85–127.
- Hill, S., Dragoset, B., Weglein, A., 1999. An introduction to this special section: the new world of multiple attenuation. *The Leading Edge* 18 (1), 38–136.
- Jackson, M.P.A., Vendeveille, B.C., Schultz-Ela, D.D., 1994. Salt-related structures in the Gulf of Mexico: a field guide for geophysicists. *The Leading Edge* 13 (8), 837–842.
- Jansson, P., 1997. *Deconvolution of Images and Spectra*, second ed. Academic Press Inc., Orlando, FL, USA 514pp.
- Lambará, G., Lucio, P.S., Hanyga, A., 1996. Two-dimensional multivalued traveltime and amplitude maps with uniform ray density criterion. *Geophysical Journal International* 125, 584–598.
- Lecomte, I., 2006. Illumination, resolution, and incidence-angle in PSDM: a tutorial. In: *Expanded Abstracts of the 76th Annual International Meeting of the Society of Exploration Geophysicists*, New Orleans, LA, USA, pp. 2544–2548.
- Lecomte, I., 2008. Resolution and illumination analyses in PSDM: a ray-based approach. *The Leading Edge* 27 (5), 650–663.
- Lecomte, I., Gelius, L.J., 1998. Have a look at the resolution of prestack depth migration for any model, survey and wavefields. In: *Expanded Abstracts of the 68th Annual International Meeting of the Society of Exploration Geophysicists*, New Orleans, LA, USA, pp. 1112–1115.
- Lecomte, I., Gjøystdal, H., Drottning, Å., 2003. Simulated prestack local imaging: a robust and efficient interpretation tool to control illumination, resolution, and time-lapse properties of reservoirs. In: *Expanded Abstracts of the 73rd Annual International Meeting of the Society of Exploration Geophysicists*, Dallas, TX, USA, pp. 1525–1528.
- Loewenthal, D., Lu, L., Roberson, R., Sherwood, J., 1976. The wave equation applied to migration. *Geophysical Prospecting* 24 (2), 380–399.
- Margave, G.F., 2001. *Numerical Methods of Exploration Seismology with Algorithms in MATLAB*. The University of Calgary <<http://www.crewes.org/>> (Accessed 18 January 2008).
- Matson, K., Dragoset, B., 2005. An introduction to this special section—multiple attenuation. *The Leading Edge* 24 (3), 252–318.
- Norman, H.J., 2001. *Nontechnical Guide to Petroleum Geology Exploration Drilling and Production*, second ed. PennWell Books, Tulsa, OK, USA 575pp.
- Popovici, A.M., 1994. Reducing artifacts in prestack phase-shift migration of common-offset gathers. In: *Expanded Abstracts of the 64th Annual International Meeting of the Society of Exploration Geophysicists*, Los Angeles, CA, USA, pp. 684–687.
- Pratson, L., Gouveia, W., 2002. Seismic simulations of experimental strata. *Bulletin of the AAPG* 86 (1), 129–144.
- Schuster, G.T., Hu, J., 2000. Green's function for migration: continuous recording geometry. *Geophysics* 65 (1), 167–175.
- Sheriff, R.E., 2001. *Encyclopedic Dictionary of Applied*, fourth ed. Geophysics, Society of Exploration Geophysicists, Tulsa, OK, USA, 429pp.
- Stockwell, J.W., 1999. The cwp/su: Seismic un*x package. *Computers & Geosciences* 25 (4), 415–419.
- Streich, R., van der Kruk, J., Green, A.G., 2007. Vector-migration of standard copolarized 3D GPR data. *Geophysics* 72 (5), J65–J75.
- Thorbecke, J., Wapenaar, K., Swinnen, G., 2004. Design of one way wavefield extrapolation operators, using smooth functions in WLSQ optimization. *Geophysics* 69 (4), 1037–1045.
- Toxopeus, G., Petersen, S.A., Wapenaar, K., 2003a. Improving geological modeling and interpretation by simulated migrated seismic. In: *Extended Abstracts of the 65th Meeting of the European Association of Geoscientists and Engineers*, Stavanger, Norway, p. F34.
- Toxopeus, G., Slob, E., Draijer, M., 2003b. E-Learning for geoscience: an educational approach. *First Break* 21 (8), 45–48.
- Toxopeus, G., Thorbecke, J., Wapenaar, K., Petersen, S., Slob, E., Fokkema, J., 2008. Simulating migrated and inverted seismic data by filtering a geologic model. *Geophysics* 73 (2), T1–T10.
- Verschuur, D.J., Berkhout, A.J., Wapenaar, C.P.A., 1992. Adaptive surface-related multiple elimination. *Geophysics* 57 (9), 1166–1177.
- Wapenaar, C.P.A., Berkhout, A.J., 1989. *Elastic Wave Field Extrapolation: Redatuming of Single and Multi-component Seismic Data*. Elsevier Science Publishing Co., Amsterdam, New York 468pp.
- Widess, M.B., 1973. How thin is a thin bed? *Geophysics* 38 (6), 1176–1180.
- Xie, X.B., Jin, S., Wu, R.S., 2006. Wave-equation-based seismic illumination analysis. *Geophysics* 71 (5), S169–S177.
- Yang, H., Xie, X.-B., Luo, M., Jin, S., 2008. Target oriented full-wave equation based illumination analysis. In: *Expanded Abstracts of the 74th Annual International Meeting of the Society of Exploration Geophysicists*, Las Vegas, NV, USA, pp. 2216–2220.
- Yilmaz, O., 2001. *Seismic Data Analysis*. Society Of Exploration Geophysicists, Tulsa, OK, USA 2027pp.
- Zhu, J., Lines, L., Gray, S., 1998. Smiles and frowns in migration/velocity analysis. *Geophysics* 63 (4), 1200–1209.